

Graphene under extreme electromagnetic field: energetic ion acceleration by direct irradiation of ultra intense laser on few layer suspended graphene

Yasuhiro Kuramitsu (✉ kuramitsu@eei.eng.osaka-u.ac.jp)

Osaka University <https://orcid.org/0000-0002-0160-2260>

Takumi Minami

Osaka University

Takamasa Hihara

Osaka University

Kentaro Sakai

Osaka University

Takahiro Nishimoto

Osaka University

Shogo Isayama

Kyushu University

Yu-Tzu Liao

National Central University

Kuan-Ting Wu

National Central University

Wei-Yen Woon

National Central University <https://orcid.org/0000-0001-7299-9122>

Shih-Hung Chen

National Central University

Yao-Li Liu

National Central University

Shi-Ming He

National Central University

Ching-Yuan Su

National Central University <https://orcid.org/0000-0001-9295-7587>

Masato Ota

Osaka University

Shunsuke Egashira

Osaka University

Alessio Morace

Osaka University

Youichi Sakawa

Osaka University

Hideaki Habara

Osaka University <https://orcid.org/0000-0002-7697-6830>

Ryosuke Kodama

Osaka University

Leonard Dohl

University of York

Nigel Woolsey

University of York <https://orcid.org/0000-0002-2444-9027>

Michel Koenig

Ecole Polytechnique

Masato Kanasaki

Kobe University

Takafumi Asai

Kobe University

Tomoya Yamauchi

Kobe University

Keiji Oda

Kobe University

Kotaro Kondo

QST/KPSI

Hikomitsu Kiriama

QST/KPSI

Yuji Fukuda

QST/KPSI <https://orcid.org/0000-0002-1348-0483>

Article

Keywords: graphene, electromagnetic field, energetic ion acceleration

Posted Date: June 17th, 2021

DOI: <https://doi.org/10.21203/rs.3.rs-373515/v1>

License:  This work is licensed under a Creative Commons Attribution 4.0 International License.

[Read Full License](#)

Graphene under extreme electromagnetic field: energetic ion acceleration by direct irradiation of ultra intense laser on few layer suspended graphene

(Dated: April 18, 2021)

Atomically thin graphene is a transparent, highly electrically and thermally conductive, light-weight, and the strongest material [1–3]. To date, graphene has found applications in many aspects including transport, medicine, electronics, energy, defense, and desalination [4–10]. We demonstrate another disruptive application of graphene in the field of laser-ion acceleration, in which the unique features of graphene play indispensable role. Laser driven ion sources have been widely investigated for pure science, plasma diagnostics, medical and engineering applications [11]. Recent developments of laser technologies allow us to access radiation regime [12–14] of laser ion acceleration with relatively thin targets [15–19]. However, the thinner target is the less durable and can be easily broken by the pedestal or pre-pulse through impact and heating prior to the main laser arrival [20, 21]. One of the solutions to avoid this is plasma mirror, which is a surface plasma created by the foot of the laser pulse on an optically transparent material working as an effective mirror only for the main laser peak. So far diamond like carbon (DLC) is used to explore the ion acceleration in extremely thin target regime (< 10 nm) with plasma mirrors [15], and it is necessary to use plasma mirrors even in moderately thin target regime (10–100 nm) to realize energetic ion generation [16–19]. However, firstly DLC is not 2D material, and therefore, it is very expensive to make it thin and flat. Moreover, graphene is stronger than diamond at extremely thin regime [2], and much more reasonable for mass-production. Furthermore, installing and operating plasma mirrors at high repetition rate is also costly. Here we show another direct solution using graphene as the thinnest and strongest target ever made. We develop a facile transfer method to fabricate large-area suspended graphene (LSG) as target for laser ion acceleration with precision down to a single atomic layer [22]. Direct irradiation of the LSG targets with an ultra intense laser generates energetic carbons and protons evidently showing the durability of graphene without plasma mirror. This extends the new frontier of science on graphene under extreme electromagnetic field, such as energy frontier and nuclear fusion.

The experiments are performed with the J-KAREN-P laser at the short-F chamber, Kansai Photon Science Institute in Japan [25], where the laser intensity reaches

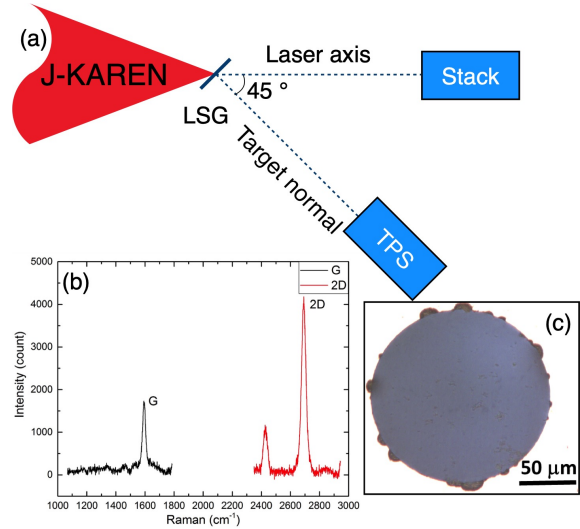


FIG. 1. (a) Schematic setup of the experiment with the large-area suspended graphene target (LSG). The J-KAREN-P laser is focused with an F/1.3 off-axis parabolic mirror (OAP) on the LSG from 45 degrees to the target normal direction to avoid the back reflection of incident light to destroy the upstream optics, without plasma mirror. The pulse energy, duration, focal spot and the intensity are ~ 10 J on target, 40 fs, $\sim 2\mu\text{m}$, and $\sim 5 \times 10^{21} \text{ Wcm}^{-2}$, respectively, measured just before the experiment. (b) and (c) shows the Raman spectrum and the optical microscope image for a typical LSG, respectively; from which the narrow bandwidth of 2D band ($< 30 \text{ cm}^{-1}$) and the higher intensity ratio (> 2.5) of the 2D and G bands ($I(2D)/I(G)$) confirmed the presence of single-layer LSG [23, 24]. The small peak next to the 2D peak comes from the tiny curvature of LSG due to the large aspect ratio of LSG. We place the convex and concave side to the laser and detector, respectively, for the better beam collimation. Note that the ideal LSG is 0.34 nm, while the obtained transferring graphene is close to 1 nm due to molecular adsorption on the surface [22]. By transferring graphene layer by layer, we control the target thickness at 1 nm accuracy [22]. The accelerated ions are detected with a stack of radiochromic films (RCFs) and solid state nuclear track detector (CR-39) and Thomson parabola spectrometer.

the highest class currently available in the world. Figure 1 (a) shows the schematic images of experimental setup, and the specification of laser is provided in the caption. By irradiating the LSGs with the intense lasers, energetic ion beams are produced. The ion diagnostics are stack detector composed of radiochromic films (RCF) and solid state nuclear track detectors (CR-39), where the higher energy ions can penetrate through the deeper, and Thomson parabola spectrometer (TPS) described in Supplementary Figure 1. When a solid target is irradi-

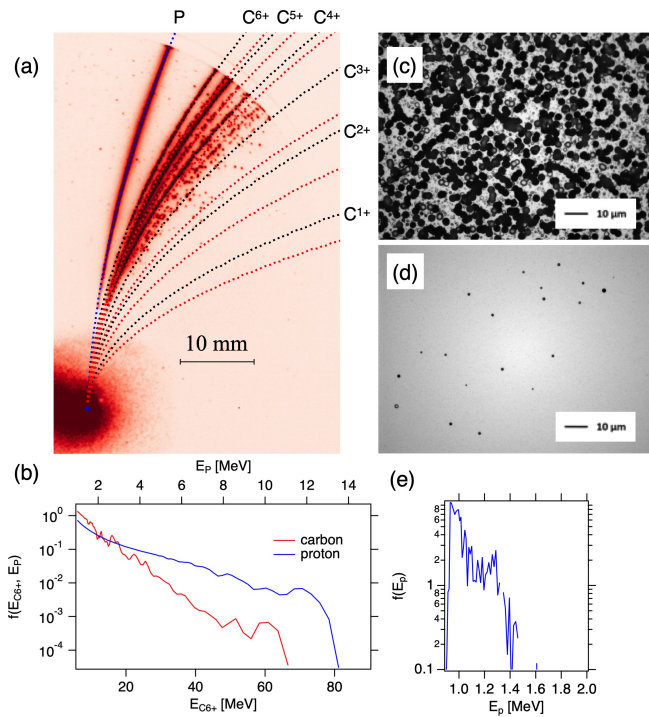


FIG. 2. (a) Image obtained with TPS with 8-layer LSG, where a micro-channel plate (MCP) and CCD are used as detector. The electric and magnetic fields displace the ion trajectories depending on the charge to mass ratio (as shown in Supplementary Figure 1). The black and green parabolae correspond to carbon and oxygen ions, respectively. Note that C^{6+} (C^{3+}) overlaps with O^{8+} (O^{4+}). The plus mark in the dark feature corresponds to the zero displacement determined from the shots without target. (b) Energy distribution functions calculated from (a) for proton and C^{6+} , normalized as $\int f dE = 1$ with 8-layer LSG. The top and bottom axes show the proton and carbon energy, where the top axis is adjusted as $1/6$ of carbon energy. The ion pits on CR-39 in stack detector: (c) the carbon pits on the first CR-39 covered with a $12 \mu\text{m}$ aluminum foil with the energy range between 12 and 94 MeV, and (d) the proton pits on the CR-39 behind the aluminum foil, two RCFs, and a CR-39 corresponding to the energy of $12.2 \sim 13.2$ MeV. The ion stopping energies are calculated with the PHITS code [26]. (e) The proton energy distribution function obtained with 2-layer LSG with the incident laser angle of 10 degrees between laser axis and the target normal. We keep the TPS position as in (a).

ated with an intense laser, a proton beam is generated independent of target material due to the surface contamination from moisture in the air. The CR-39s allow us to distinguish heavier ions or mostly carbons, as confirmed in Supplementary Figure 2, from protons by the size of ion pits. Furthermore, TPS provides charge-to-mass ratio together with the energy spectra (Supplementary Figure 1).

Figure 2 shows the results of 8-layer LSG, i.e., 8 nm thick target with full energy of J-KAREN-P at the best focus. In Fig. 2 (a), the raw data of TPS is shown with

the blue, black, and red dotted lines corresponding to proton, carbon, and oxygen, respectively. Figure 2 (b) shows the proton and carbon energy distribution functions $f(E_{P,C})$, where $E_{P,C}$ are the proton and C^{6+} after subtracting the background as shown in Supplementary Figure 1. There are also about 30% oxygen ions as shown in Supplementary Figure 2. The ion spectra show bump-on-tail or monoenergetic features in higher energy tails. When the proton and carbon are accelerated by the same potential field, which is most of the case in laser ion acceleration, the carbon energy is 6 times larger than that of proton due to the difference of charge-to-mass ratio. The experimental results show the proton energy is slightly higher than $1/6$ of carbon energy. Figures 2 (c) and (d) show the etched pits of mostly carbons and protons, respectively, which is consistent with TPS. Figure 2 (e) shows the same plot as Fig. 2 (b) except with double-layer LSG corresponding to 2 nm thickness. This shot is taken on a different conditions where the laser incident angle of 10 degrees with moderate contrast level of $\sim 10^{-7}$, while for the 8-layer LSG shot it is $\sim 10^{-10}$ or better [25]. Since the geometry of the tight focus laser with $F/1.3$, a hole on a substrate to suspend graphene has to be big enough not to irradiate the inner side of the hole. We use $400 \mu\text{m}$ hole for safety with the 45 degrees incidence. The success rate to make the single and double-layer graphene suspended over $400 \mu\text{m}$ hole is still low, and we just use $200 \mu\text{m}$ hole for double-layer LSG here. As mentioned above, the pre-pulse and pedestal are major practical problem in the extremely thin target regime and the recent experiments[15–19] all utilize the single or double plasma mirrors to suppress the pre-pulse and pedestal to realize the energetic ion acceleration. It is astonishing that the energetic ions are generated by irradiating the single figure nanometer thin targets with the ultra intense laser at $\sim 10^{22} \text{ Wcm}^{-2}$ without plasma mirror. Our double-layer LSG is the thinnest target ever generate the energetic ions and even without plasma mirror at this thickness.

Figures 3 (a) and (b) show the schematic setup for the transmission/reflection measurements with weak laser and the results, respectively. As indicated in Supplementary Figure 2, the LSG contains the contaminants as water molecules. We measure the transmission (T) and reflection rates (R), and obtain the absorption rate (A) by $A = 100 - (T + R)$. The transmission power is measured with and without graphene, and thus, most reliable and the error is also small as shown in Fig. 3 (b). As the reflection power is weak, the error bars on the reflectivity is large as for the absorption. It is known that a single atomic layer graphene absorbs white light $A = 2.3\%$ defined by the fine structure constant [28], and that the graphene is highly transparent ($T \sim 97.7\%$) and the reflectivity is negligibly small ($R < 0.1\%$) [27, 29]. We plot the 97.7% transmission (blue dotted) and 2.3% absorption (red dotted) per layer for reference in Fig. 3 (b).

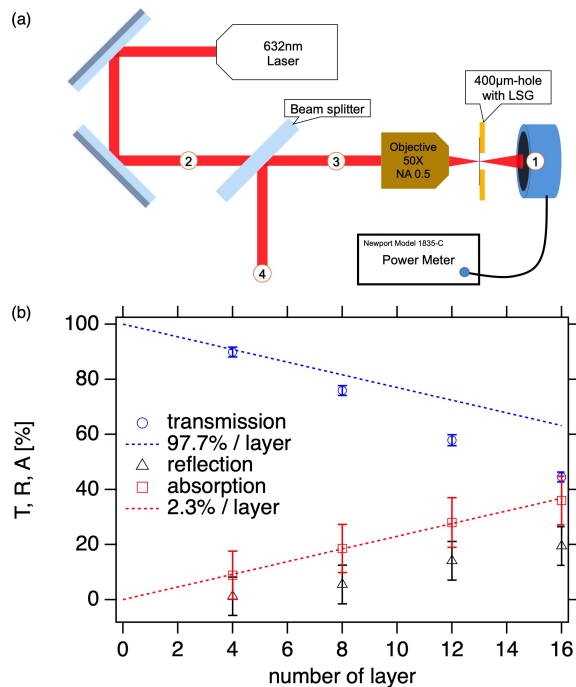


FIG. 3. (a) Schematic image of setup for the LSG transmission/reflection measurement. We use a He-Ne laser with wavelength of 632 nm and focus the beam with an objective lens with the numerical aperture of 0.5 on to the LSG suspended over 400 μm hole. Measuring the laser powers at position 1, the transmission rate T can be calculated by dividing the results with and without LSGs on the 400 μm hole. To acquire accurate reflection rate R , the optical properties of the beam splitter (T_s, R_s) and the lens (T_l, R_l) are obtained in advance with the focused beam passing through an empty hole. Provided the laser power measured at position 2 is P , the laser power measured at position 4 is $PT_sT_l^2RR_s + PT_sR_lR_s$, from which R can be derived. (b) The transmission (T), reflection (R), and absorption rates (A) are plotted against the number of layer of LSG. The error bars represent the standard deviation of the measurements. The dotted lines represent the theoretical transmission (blue) and absorption rates (red) [27].

With 4-layer LSG, the transmission is comparable to the ideal value of 97.7% transmission per layer. The transmission deviates from the blue line as the number of layer increases. The reflection rate also increases as the number of layer increases; it is not negligible for many layer LSGs. The measured absorption rate excellently agrees with the theoretical line of 2.3% absorption per layer. This indicates that the contaminants reflect the light but not absorb it at low intensity light. There are two significant outcome of LSG when used as targets for laser-driven ion sources; 1. The light exerts pressure only on the contaminants until the LSG is ionized, and 2. most of the laser power (97.7%) is not absorbed by LSG until the LSG is ionized, where only 2.3% laser power is absorbed and can convert to heat causing the LSG melting prior to the main laser peak. Furthermore, the thermal

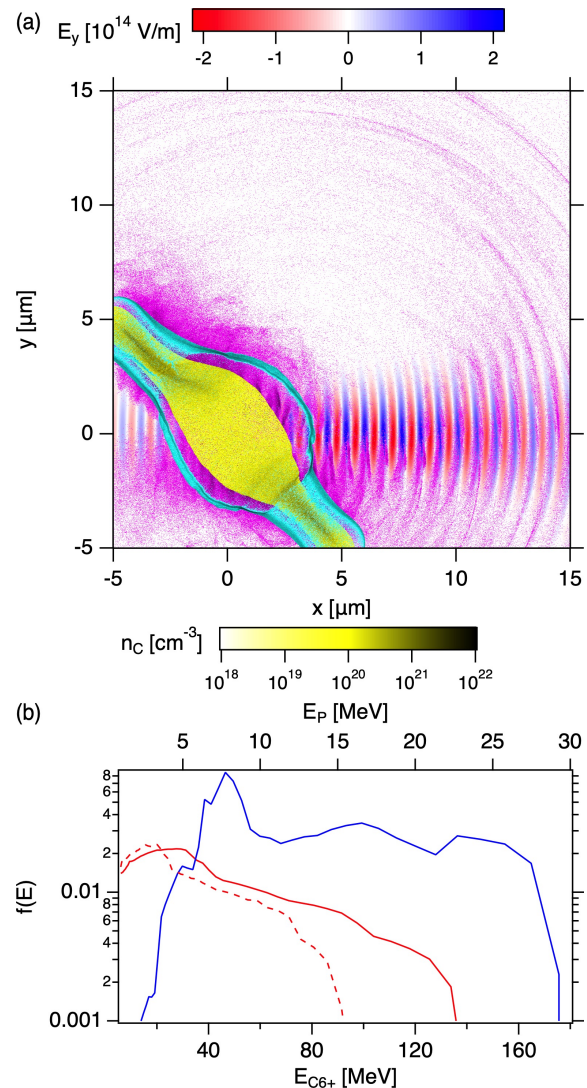


FIG. 4. (a) The snapshots from 2D Particle-in-cell (PIC) simulation at ~ 20 fs from the laser peak arrival at the 8 layer LSG target. The laser electric field E_y (blue-red), electron n_e (magenta), carbon n_C (yellow), and proton number densities n_p (cyan) are overlaid. The color scales for the number densities are set to be identical. The laser pedestal and pre-pulse are not taken into account. (b) The same as Fig. 2 (b) except calculated from the PIC simulation with all the particles in the simulation box, where red and blue solid lines represent carbon and proton, respectively. The maximum ion energies are higher than that of experiment. The dashed line shows the carbon spectrum with pure LSG with pre-ionization and 10 times expansion, i.e. 80 nm thick with 0.1 n_C . The time 0 corresponds to the laser peak arrival at the target.

conductivity of graphene is extremely high [3], and thus, the heat can diffuse quicker than other materials within the layer, but not for interlayers. These significant features make the LSG durable against the pre-pulse and pedestal. Graphene is an ultimate material not only for target for laser driven ion sources but also for plasma mirrors.

We perform 2D particle-in-cell (PIC) simulations with an open code EPOCH [30]. Figure 4 (a) shows the snapshot of 2D simulation at 20 fs from the laser peak arrival at the target with the target ionization by laser. We estimate the total number of electrons from LSG including water contaminations, and then replace the oxygen with carbon for simplicity; the major component of heavy ions are essentially from graphene carbons as shown in Supplementary Figure 2. The simulation details are given in the Supplementary information. In Fig. 4 (a) the lightest electrons (magenta) are firstly accelerated by the laser electric field, and then, the second lightest protons (cyan) follow due to the space charge effect. The protons are localized in thin layers even though the protons distribute randomly in space within the target and mixed with carbons in the initial condition. The proton energy is comparable but higher than the 1/6 of carbon energy as in Fig. 4 (b). As seen in the experimental results in Fig. 2 (b), there is also a bump on tail in the proton energy distribution function for $E_P \sim 140 - 160$ MeV in Fig. 4 (b) although it is not clear for carbon. This indicates the thin structures of protons correspond to the localization in energy space since they are moving together. In case of experiment, we measure the ions from target normal direction, which is 45 degrees from the laser axis. This results in the enhancement of monoenergetic feature. The numerical results are qualitatively consistent with the experiment, and quantitatively just factor two overestimated. This indicates that the target is ionized before the main laser peak arrival in the experiment due to the pre-pulse and pedestal.

As shown in Supplementary Figure 3, by assuming the pre-ionization of the targets due to the pre-pulse and pedestal, the expanded targets keeping the total number of particles same result in smaller ion energies as in the experiment. Our experimental and numerical results show that the LSGs are melted but still keep the critical density. Another possibility account for the lower experimental results is that the LSG optical properties show in Fig. 3. We consider the homogeneous expansion including the electrons from the contaminants, however, as discussed above, the weak light pressure before the ionization of graphene can act only on the contaminants. Therefore, we simply consider the pure graphene density with pre-ionized expanded target by factor 10 with the reduced density. The carbon energy is still slightly higher than but comparable to the experimental energies as shown with the dashed line in Fig. 3. Note that there is no comprehensive numerical code that includes the quantum electrodynamics-molecular dynamics together with the corrective plasma dynamics. Our results imply the necessity of such code. This will be discussed elsewhere in the future.

In summary, we have developed an extremely thin target, large-area suspended graphene (LSG), which is the thinnest, lightest, transparent, and strongest target. By

transferring graphene layer by layer, we control the target thickness by 1 nm accuracy. We measured the LSG transmission, reflection, and absorption rates, where the transmission and reflection deviate from the theoretical prediction, however, the absorption rate is nearly identical to the theoretical expectation of 2.3% per layer. By irradiating the LSGs with J-KAREN-P without plasma mirror, we observed energetic protons and carbons. The double-layer LSG is the thinnest target that has ever actually produced energetic ions with intense lasers. We also perform 2D PIC simulations with various conditions; the numerical results are qualitatively and quantitatively consistent with the experimental results. This clearly shows that even though the graphene is melted by pre-pulse, it can keep the critical density at $\sim 10^{22}$ Wcm⁻² without plasma mirror. Furthermore, our experimental and numerical results show that the target thickness is still too thin, and also that we do not need that high intensity to produce several MeV ions. As shown in Supplementary Figure 2 the defocused low energy J-KAREN-P laser at $\sim 10^{17}$ Wcm⁻² can generate several MeV protons and carbons; table-top lasers can be also used to generate the several MeV ions at high repetition rates with LSGs. Our results also indicates that the thicker LSG with plasma mirror is promising to explore the energy frontier of laser-driven energetic ions.

-
- [1] C. Lee, X. Wei, J. W. Kysar, and J. Hone, *Science* **321**, 385 (2008).
 - [2] J.-H. Lee, P. E. Loya, J. Lou, and E. L. Thomas, *Science* **346**, 1092 (2014).
 - [3] A. A. Balandin, S. Ghosh, W. Bao, I. Calizo, D. Teweldebrhan, F. Miao, and C. N. Lau, *Nano Letters* **8**, 902 (2008).
 - [4] E. J. Siochi, *Nature Nanotechnology* **9**, 745 EP (2014).
 - [5] S. Chen, L. Brown, M. Levendorf, W. Cai, S.-Y. Ju, J. Edgeworth, X. Li, C. W. Magnuson, A. Velamakanni, R. D. Piner, J. Kang, J. Park, and R. S. Ruoff, *ACS Nano*, *ACS Nano* **5**, 1321 (2011).
 - [6] Y. Li, H. Yuan, A. von dem Bussche, M. Creighton, R. H. Hurt, A. B. Kane, and H. Gao, *Proceedings of the National Academy of Sciences of the United States of America* **110**, 12295 (2013).
 - [7] S. Bae, H. Kim, Y. Lee, X. Xu, J.-S. Park, Y. Zheng, J. Balakrishnan, T. Lei, H. Ri Kim, Y. I. Song, Y.-J. Kim, K. S. Kim, B. Özyilmaz, J.-H. Ahn, B. H. Hong, and S. Iijima, *Nature Nanotechnology* **5**, 574 EP (2010).
 - [8] T.-H. Han, Y. Lee, M.-R. Choi, S.-H. Woo, S.-H. Bae, B. H. Hong, J.-H. Ahn, and T.-W. Lee, *Nature Photonics* **6**, 105 EP (2012).
 - [9] X. Yang, C. Cheng, Y. Wang, L. Qiu, and D. Li, *Science* **341**, 534 (2013).
 - [10] D. Cohen-Tanugi and J. C. Grossman, *Nano Letters*, *Nano Letters* **12**, 3602 (2012).
 - [11] A. Macchi, M. Borghesi, and M. Passoni, *Reviews of Modern Physics* **85**, 751 (2013).
 - [12] T. Esirkepov, M. Borghesi, S. V. Bulanov, G. Mourou,

- and T. Tajima, *Physical Review Letters* **92**, 175003 (2004).
- [13] A. P. L. Robinson, M. Zepf, S. Kar, R. G. Evans, and C. Bellei, *New Journal of Physics* **10**, 013021 (2008).
- [14] A. Macchi, S. Veghini, and F. Pegoraro, *Phys. Rev. Lett.* **103**, 085003 (2009).
- [15] A. Henig, S. Steinke, M. Schnürer, T. Sokollik, R. Hörlein, D. Kiefer, D. Jung, J. Schreiber, B. M. Hegelich, X. Q. Yan, J. Meyer-Ter-Vehn, T. Tajima, P. V. Nickles, W. Sandner, and D. Habs, *Physical Review Letters* **103**, 245003 (2009).
- [16] S. Kar, K. F. Kakolee, B. Qiao, A. Macchi, M. Cerchez, D. Doria, M. Geissler, P. McKenna, D. Neely, J. Osterholz, R. Prasad, K. Quinn, B. Ramakrishna, G. Sarri, O. Willi, X. Y. Yuan, M. Zepf, and M. Borghesi, *Physical Review Letters* **109**, 185006 (2012).
- [17] S. Steinke, P. Hilz, M. Schnürer, G. Priebe, J. Bränzel, F. Abicht, D. Kiefer, C. Kreuzer, T. Ostermayr, J. Schreiber, A. A. Andreev, T. P. Yu, A. Pukhov, and W. Sandner, *Phys. Rev. ST Accel. Beams* **16**, 011303 (2013).
- [18] I. J. Kim, K. H. Pae, I. W. Choi, C.-L. Lee, H. T. Kim, H. Singhal, J. H. Sung, S. K. Lee, H. W. Lee, P. V. Nickles, T. M. Jeong, C. M. Kim, and C. H. Nam, *Physics of Plasmas* **23**, 070701 (2016).
- [19] C. Scullion, D. Doria, L. Romagnani, A. Sgattoni, K. Naughton, D. R. Symes, P. McKenna, A. Macchi, M. Zepf, S. Kar, and M. Borghesi, *Physical Review Letters* **119**, 054801 (2017).
- [20] M. Borghesi, *Nuclear Instruments and Methods in Physics Research Section A: Accelerators, Spectrometers, Detectors and Associated Equipment* **740**, 6 (2014), proceedings of the first European Advanced Accelerator Concepts Workshop 2013.
- [21] G. M. Petrov, C. McGuffey, A. G. R. Thomas, K. Krushelnick, and F. N. Beg, *Journal of Applied Physics* **119**, 053302 (2016).
- [22] N. Khasanah, N. Bolouki, T.-Y. Huang, Y.-Z. Hong, W.-L. Chung, W.-Y. Woon, C.-Y. Su, and Y. Kuramitsu, *High Power Laser Science and Engineering* **5**, e18 (2017).
- [23] A. C. Ferrari, J. C. Meyer, V. Scardaci, C. Casiraghi, M. Lazzeri, F. Mauri, S. Piscanec, D. Jiang, K. S. Novoselov, S. Roth, and A. K. Geim, *Phys. Rev. Lett.* **97**, 187401 (2006).
- [24] Y.-M. Chen, S.-M. He, C.-H. Huang, C.-C. Huang, W.-P. Shih, C.-L. Chu, J. Kong, J. Li, and C.-Y. Su, *Nanoscale* **8**, 3555 (2016).
- [25] H. Kiriya, Y. Miyasaka, A. Sagisaka, K. Ogura, M. Nishiuchi, A. S. Pirozhkov, Y. Fukuda, M. Kando, and K. Kondo, *Opt. Lett.* **45**, 1100 (2020).
- [26] T. Sato, Y. Iwamoto, S. Hashimoto, T. Ogawa, T. Furuta, S. ichiro Abe, T. Kai, P.-E. Tsai, N. Matsuda, H. Iwase, N. Shigyo, L. Sihver, and K. Niita, *Journal of Nuclear Science and Technology* **55**, 684 (2018).
- [27] S. Pang, Y. Hernandez, X. Feng, and K. Müllen, *Advanced Materials* **23**, 2779 (2011).
- [28] R. R. Nair, P. Blake, A. N. Grigorenko, K. S. Novoselov, T. J. Booth, T. Stauber, N. M. R. Peres, and A. K. Geim, *Science* **320**, 1308 (2008).
- [29] S.-E. Zhu, S. Yuan, and G. C. A. M. Janssen, *EPL (Europhysics Letters)* **108**, 17007 (2014).
- [30] T. D. Arber, K. Bennett, C. S. Brady, A. Lawrence-Douglas, M. G. Ramsay, N. J. Sircombe, P. Gillies, R. G. Evans, H. Schmitz, A. R. Bell, and C. P. Ridgers, *Plasma Physics and Controlled Fusion* **57**, 113001 (2015).

Competing interests

The authors declare no competing interests.

Data availability

The data sets generated during and/or analyzed during the current study are available from the corresponding author on reasonable request.

Supplementary Files

This is a list of supplementary files associated with this preprint. Click to download.

- [jkaren21natsupplementary.pdf](#)